

Stochastic scattering theory for excitation induced dephasing: Time-dependent nonlinear coherent exciton lineshapes

Ajay Ram Srimath Kandada,¹ Hao Li,^{2, a)} Félix Thouin,³ Eric R. Bittner,^{2, b)} and Carlos Silva^{3, 4, 5, c)}

¹⁾*Department of Physics and Center for Functional Materials, Wake Forest University, 1834 Wake Forest Road, Winston-Salem, North Carolina 27109, United States*

²⁾*Department of Chemistry, University of Houston, Houston, Texas 77204, United States*

³⁾*School of Physics, Georgia Institute of Technology, 837 State Street, Atlanta, Georgia 30332, United States*

⁴⁾*School of Chemistry and Biochemistry, Georgia Institute of Technology, 901 Atlantic Drive, Atlanta, Georgia 30332, United States*

⁵⁾*School of Materials Science and Engineering, Georgia Institute of Technology, North Avenue, Atlanta, Georgia 30332, United States*

(Dated: 29 September 2020)

We develop a stochastic theory that treats time-dependent exciton-exciton s -wave scattering and that accounts for dynamic Coulomb screening, which we describe within a mean-field limit. With this theory, we model excitation-induced dephasing effects on time-resolved two-dimensional coherent optical lineshapes and we identify a number of features that can be attributed to the many-body dynamics occurring in the background of the exciton, including dynamic line narrowing, mixing of real and imaginary spectral components, and multi-quantum states. We test the model by means of multidimensional coherent spectroscopy on a two-dimensional metal-halide semiconductor that hosts tightly bound excitons and biexcitons that feature strong polaronic character. We find that the exciton nonlinear coherent lineshape reflects many-body correlations that give rise to excitation-induced dephasing. Furthermore, we observe that the exciton lineshape evolves with population time over time windows in which the population itself is static, in a manner that reveals the evolution of the multi-exciton many-body couplings. Specifically, the dephasing dynamics slow down with time, at a rate that is governed by the strength of exciton many-body interactions and on the dynamic Coulomb screening potential. The real part of the coherent optical lineshape displays strong dispersive character at zero time, which transforms to an absorptive lineshape on the dissipation timescale of excitation-induced dephasing effects, while the imaginary part displays converse behavior. Our microscopic theoretical approach is sufficiently flexible to allow for a wide exploration of how system-bath dynamics contribute to linear and non-linear time-resolved spectral behavior.

I. INTRODUCTION

It is well recognized that many-body phenomena have a profound effect on the linear and non-linear optical lineshapes of semiconductors with reduced dimensionality, in which Coulomb correlations can be particularly strong due to decreased screening and quantum confinement effects. One such effect is biexciton formation, in which Coulomb binding of two electron-hole pairs results in new two-electron, two-hole quasiparticles.^{1–11} Another important process that is highly relevant in exciton quantum dynamics is excitation induced dephasing (EID),^{12–27} primarily investigated in two-dimensional (2D) systems such as III-V quantum wells,^{13,18–20,22–24} single-layer transition-metal dichalcogenides,^{25,26} and two-dimensional metal-halide perovskite derivatives.²⁷ This can be described as the incoherent Coulomb elastic scattering between multiple excitons or between excitons and an electron-hole plasma generated with the excitation optical field. The scattering process gives rise to faster dephasing dynamics compared to the low-density pure-dephasing limit, and may be the dominant dephasing pathway at sufficiently high densities. In many systems, espe-

cially those with strong exciton-phonon coupling, the background excitations are transient and co-evolve with optical modes of the system and consequently a strictly incoherent kinetic description such as this mesoscopic approach or a kinetic Markovian Boltzmann-like scattering theory¹⁵ cannot describe coherence dynamics. EID can be effectively rationalized from a mesoscopic perspective by means of the optical Bloch equations, which capture the effect of many-body exciton scattering on both population and coherence dynamics derived from coherent spectroscopy of semiconductors.^{20,21} Recent advances towards a more microscopic perspective have been presented by Katsch et al., in which excitonic Heisenberg equations of motion are used to describe linear excitation line broadening in two-dimensional transition-metal dichalcogenides.²⁸ Their results indicate exciton-exciton scattering from a dark background as a dominant mechanism in the power-dependent broadening EID and sideband formation. Similar theoretical modelling on this class of materials and their van der Waals bilayers have yielded insight into the role of effective mass asymmetry on EID processes.²⁹ These modelling works highlight the need for microscopic approaches to understand nonlinear quantum dynamics of complex 2D semiconductors, but the computational expense could become considerable if other many-body details such as polaronic effects are to be included.³⁰ As an alternative general approach, an analytical theory of dephasing in the same vein as Anderson-Kubo lineshape theory,^{31,32} but that includes *transient* EID and Coulomb screening effects, would be valuable

^{a)}HL and ARSK contributed equally and are first co-authors of this article.

^{b)}Electronic mail: ebittner@central.uh.edu

^{c)}Electronic mail: carlos.silva@gatech.edu

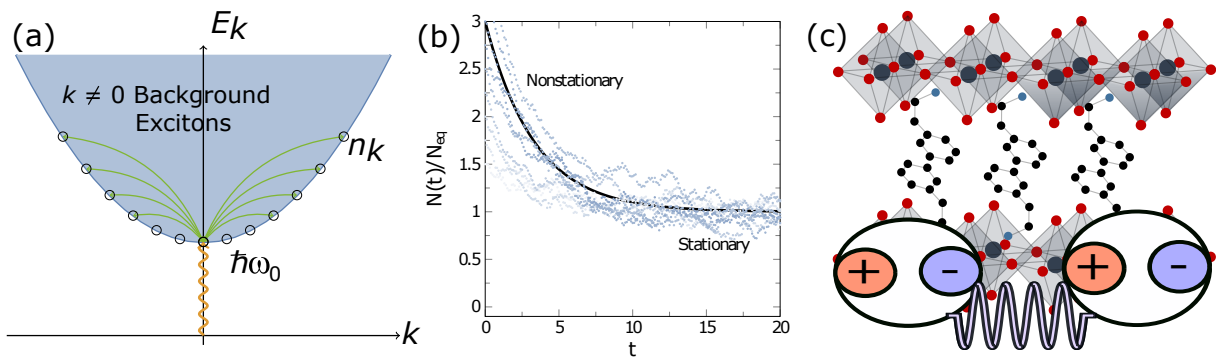


FIG. 1. (a) Schematic representation of optical absorption of excitons and exciton-exciton scattering with a background population, where the dispersion relation is in the exciton representation and $\vec{k} = \vec{k}_e + \vec{k}_h$ is the exciton wavevector. (b) Time evolution of population $N(t)/N_{\text{eq}}$ from an initial nonstationary state produced by exciton injection. Individual trajectories are represented by blue dots. Asymptotically, the function reaches a stationary state that yields the Anderson-Kubo limit. (c) Crystal structure of $(\text{PEA})_2\text{PbI}_4$ with schematic representation of Coulomb-correlated exciton-exciton elastic scattering.

to extract microscopic detail on screened exciton-exciton scattering from time-dependent nonlinear coherent ultrafast spectroscopy, via direct and unambiguous measurement of the homogeneous excitation linewidth.^{33,34}

Here we employ a quantum stochastic approach, derived from a first-principles many-body theory of interacting excitons, to develop an analytical model that describes linear and nonlinear spectral lineshapes that result from exciton-exciton scattering processes, and, importantly, their dependence on population time due to the evolution of a non-stationary/non-equilibrium excitation background (see Fig. 1(a)).

Our approach is similar in spirit to the celebrated Anderson-Kubo theory^{31,32} and reduces to that in the limit of a stationary background population at sufficiently long times.³⁵ The model captures a microscopic picture of EID by integrating over the interactions of excitons produced via a well-defined coherent pathway (Fig. 2 below), and background excitons that do not have a well-defined phase relationship that is induced by the optical field, and by treating them as a non-stationary source of quantum noise. In doing so, we can directly insert the spectral density of the bath into non-linear spectral response functions and obtain fully analytical expressions for the coherent exciton lineshapes.

We implement the model to investigate the evolution of the two-dimensional coherent excitation lineshape in a polycrystalline thin film of a prototypical two-dimensional single-layer metal-halide perovskite derivative, phenylethylammonium lead iodide $[(\text{PEA})_2\text{PbI}_4]$ (see Fig. 1(c) for the crystal structure). We have selected this material as a model system because of its well-defined exciton lineshape that we have modeled quantitatively within a Wannier-Mott framework³⁶ and because it displays strong many-body phenomena — strongly bound biexcitons at room temperature,³⁷ and robust EID effects.²⁷ Furthermore, we have concluded that the primary excitations are exciton polarons^{30,38} — quasiparticles with Coulomb correlations that are renormalized by lattice dynamics via polaronic effects; both electron-hole and photocarrier-lattice correlations are ingredients of the system Hamiltonian such that the lattice dressing constitutes an in-

tegral component of its eigenstates and eigenvalues. This renders the system highly dynamically disordered such that lattice screening effects play an important role in shaping the linewidth²⁷ and in dictating nonadiabatic dynamics.³⁹ We measure the dephasing dynamics via the homogeneous linewidth extracted by means of two-dimensional coherent excitation spectroscopy.^{33,34} In our measurements, excitons generated coherently by a sequence of time-ordered and phase-matched femtosecond pulses scatter from incoherent background excitons and thereby undergo EID, which is perceived via changes of the homogeneous linewidth. We find that EID affects the complex lineshape by mixing absorptive and dispersive features in the real and imaginary spectral components; the real component of the two-dimensional coherent spectrum initially displays a dispersive lineshape that evolves into an absorptive over the timescale in which EID couplings persist, and the imaginary component evolves in the converse fashion. Furthermore, we find that the homogeneous contribution to the spectral linewidth narrows with population time, indicating a dynamic slowing down of the dephasing rate as the EID correlations active at early time dissipate. We find that the dynamic line narrowing phenomenon is reproduced by our stochastic scattering theory, which allows us to explore the effect of dynamic Coulomb screening on EID quantum dynamics.

II. THEORETICAL MODEL

A complete derivation of our stochastic scattering theory is presented in reference 35; here we outline the elements that allow us to calculate nonlinear coherent spectral lineshapes. Our model is initiated by assuming that at $t = 0$ a non-stationary population of background excitations is created by a broad-band laser excitation. This physical picture is sketched in Fig. 1. In the current work, excitation occurs with a sequence of phase-matched and time-ordered femtosecond pulses used to measure a coherent nonlinear excitation spectrum, and the excitons produced and measured via a well de-

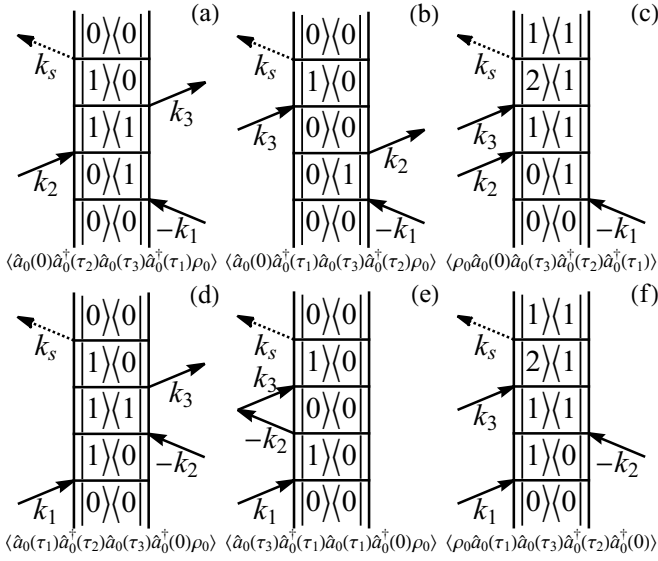


FIG. 2. Double-sided Feynman Diagrams for coherent response functions (equation 16) with rephasing phase matching (top): (a) R_{2a} , (b) R_{3a} , (c) R_{1b}^* , and non-rephasing phase matching (bottom): (d) R_{1a} , (e) R_{4a} , (f) R_{2b}^* .

finer coherent pathway (see Fig. 2 for the relevant ones in this work) are assumed to scatter elastically with their incoherent counterparts — excitons that are produced by the pulse sequence but have no phase relationship to those that produce signal in our experiments. The initial background population can be characterized by an average population N_0 and variance σ_{N_0} both of which depend upon the excitation pulse as well as the density of states of the material. Optical excitations at $k = 0$ evolve in concert with a non-stationary ($k \neq 0$) background of excitations in which the interaction determined by a screened Coulomb potential giving rise to a noisy driving term that effectively modulates the exciton energy gap. These background excitations undergo diffusion as the population relaxes to some stationary distribution. In reference 35 we show how one can arrive at a reduced model described by a Hamiltonian of the form

$$H_0(t) \approx \omega_0 \hat{a}_0^\dagger \hat{a}_0 + \frac{\gamma_1}{2} \hat{a}_0^\dagger \hat{a}_0^\dagger \hat{a}_0 \hat{a}_0 + 2\gamma_1 \hat{a}_0^\dagger \hat{a}_0 N(t), \quad (1)$$

whereby \hat{a}_0 and \hat{a}_0^\dagger are exciton operators, $N(t)$ is a stochastic variable representing the number of background excitations (see Fig. 1(b) for a depiction of its non-stationary nature), γ_1 is the exciton-exciton interaction, which we obtain from the s -wave scattering length a and reduced mass μ within the Born approximation⁴⁰

$$\gamma_1 = \frac{4\pi\hbar a}{\mu}. \quad (2)$$

This assumption does not rely upon the specific form of the exciton-exciton interaction, only that it be of finite range. In the current context, this interaction will be due to Coulomb-mediated exciton-exciton scattering that gives rise to EID.²⁷ However, it is possible that each distinct exciton within the

family of the 2D perovskite system considered here³⁰ have a distinct and unique value of γ_1 , as we reported in ref. 27, where we demonstrated distinct Coulomb screening of different exciton polarons. For purposes of our theoretical model, we assume that the system has a *single* exciton species that is susceptible to many-body scattering and therefore EID mediated via γ_1 . The exciton operators themselves then evolve as

$$\hat{a}_0(t) = \exp\left(-i(\omega_0 + \frac{\gamma_1}{2}\hat{n}_0)t - i2\gamma_1 \int_0^t N(\tau)d\tau\right)\hat{a}_0, \quad (3)$$

where $\hat{n}_0 = \hat{a}_0^\dagger \hat{a}_0$ is the number operator of $k = 0$ excitons, which is a Schrödinger operator and is therefore time independent. This development is within the framework of the interaction representation. These operators are then used to construct the expressions shown schematically in Fig. 2. Finally, it should be noted that the angle brackets $\langle \dots \rangle$ below each diagram denote both the thermal average over the initial conditions as well as averaging over the stochastic variable, $N(t)$.

A central part of our model is that we assume that the background population, $N(t) = \langle \sum_{k \neq 0} a_k^\dagger a_k \rangle$ follows from an Ornstein-Uhlenbeck process described by the stochastic differential equation

$$dN(t) = -\gamma N(t)dt + \sigma dW(t), \quad (4)$$

where $W(t)$ represents a Wiener process (continuous-time stochastic process), γ gives the background relaxation rate, and σ gives the variance. This is a reasonable assumption lacking an explicit description of the background population and its influence on the system as a source of random collisions. Ornstein-Uhlenbeck is a prototypical noisy relaxation process and describes the dynamics of an over-damped oscillator driven by thermal fluctuations.

For a stationary background population, i.e. $\langle N(t) \rangle = 0$ the covariance evolves according to $\langle N(t)N(s) \rangle = \langle N(t-s)N(0) \rangle = \sigma^2 \exp[-\gamma|t-s|]/2\gamma$. In this limit, our model reduces to the Anderson-Kubo model in which the frequency fluctuates about a stationary average according to an Ornstein-Uhlenbeck process. In this case, the population relaxation time in our model is equivalent to the correlation time in Anderson-Kubo and this gives the rate at which the environment relaxes back to its stationary average given a small push. Moreover, the fluctuation amplitude, Δ^2 , in Anderson-Kubo is equivalent to $\omega_0 \gamma_1 \sigma^2 / \gamma$ in our model. As we shall show, what appears at first to be a simple modification to the dynamics of a system has rather significant implications in terms of the non-linear spectral response of the system.

At time $t = 0$, we push the background population significantly away from the steady-state distribution to an initial value of $N(0) = N_0$, the population evolves as

$$N(t) = N_0 e^{-\gamma t} + \sigma \int_0^t e^{-\gamma(t-s)} dW(s). \quad (5)$$

and

$$\langle N(t) \rangle = e^{-\gamma t} N_0, \quad (6)$$

where N_0 is the mean number of background excitations present at time $t = 0$. In principle, there will be a distribution about this mean characterized by a variance $\sigma_{N_0}^2$. As a result, we break reversibility and the time symmetry of the correlation functions. Mathematically, this means that $\langle N(t)N(s) \rangle \neq \langle N(t-s)N(0) \rangle$ since the choice of initial time is no longer arbitrary.

In Ref. 35 we discuss the use of Itô calculus^{41–43} to evaluate these correlation functions. From a practical point of view, the Itô calculus is a tool for manipulating stochastic processes that are closely related to Brownian motion and Itô's lemma allows us to easily perform noise-averaged interactions. For the model at hand, the covariance of $N(s)$ and $N(t)$ is given by

$$\begin{aligned} \text{Cov}(N_s, N(t)) &= \langle (N_s - \langle N_s \rangle)(N(t) - \langle N(t) \rangle) \rangle \\ &= \frac{\sigma^2}{2\gamma} \left(e^{-\gamma|t-s|} - e^{-\gamma(t+s)} \right) + \sigma_{N_0}^2 e^{-\gamma(s+t)}, \end{aligned} \quad (7)$$

with $\sigma_{N_0}^2$ being the variance of $N(0)$ while the third term vanishes. Similarly, the variance

$$\text{Var}[N(t)] = \left(\sigma_{N_0}^2 - \frac{\sigma^2}{2\gamma} \right) e^{-2\gamma t} + \frac{\sigma^2}{2\gamma} \quad (8)$$

also depends upon the initial variance in the background population. Mathematically, the Fourier transform of the kernel of the integral in Eq. 5 provides the spectral density of the noisy process. In fact, a trivial modification of the approach would

be to replace the kernel in Eq. 5 with another kernel reflecting a more complex spectral density. The resulting expressions for the responses will be more complex indeed. However, Itô's lemma provides a tractable route for computing the necessary response functions.

A. Optical response functions and spectral lineshapes

Such expressions are useful since they enter directly into the calculation of response functions for linear and non-linear spectroscopy. For example, the linear response for optical excitation is given by

$$S^{(1)}(t) = \langle \hat{\mu}(t) [\hat{\mu}(0), \rho(-\infty)] \rangle, \quad (9)$$

where $\hat{\mu}(t) = \mu(\hat{a}_0^\dagger(t) + \hat{a}_0(t))$ is the excitonic transition dipole operator and $\rho(-\infty)$ is the initial density matrix. The absorption spectrum is obtained by Fourier transformation.

Averaging over the fluctuations generates terms involving cumulants of the background noise, which result in terms such as

$$\left\langle \exp \left[-i\gamma \int_0^t N(\tau) d\tau \right] \right\rangle \approx e^{i\gamma g_1(t) - \frac{\gamma^2}{2} g_2(t)}, \quad (10)$$

where $\langle \dots \rangle$ denotes averaging over noise. Here, the first cumulant $g_1(t)$ gives rise to a characteristic frequency shift as the background population decays:

$$g_1(t) = \int_0^t \langle N(\tau) \rangle d\tau = \frac{N_0}{\gamma} (1 - e^{-\gamma t}), \quad (11)$$

and

$$\begin{aligned} g_2(t, t') &= \int_0^t \int_0^{t'} \text{Cov}[N(\tau), N(\tau')] d\tau' d\tau = \\ &= \frac{\sigma^2}{2\Gamma^3} \left[2\Gamma \min(t, t') + 2e^{-\Gamma t} + 2e^{-\Gamma t'} - e^{-\Gamma|t'-t|} - e^{-\Gamma(t'+t)} - 2 \right] \\ &+ \frac{\sigma_{N_0}^2}{\Gamma^2} \left[e^{-\Gamma(t+t')} - e^{-\Gamma t} - e^{-\Gamma t'} + 1 \right]. \end{aligned} \quad (12)$$

When the two time limits are the same, this reduces to

$$\begin{aligned} g_2(t) &= \int_0^t \int_0^t \text{Cov}[N(\tau), N(\tau')] d\tau d\tau' \\ &= \frac{\sigma^2}{2\gamma^3} (2\gamma t + 4e^{-\gamma t} - e^{-2\gamma t} - 3) + \frac{\sigma_{N_0}^2}{\gamma^2} (1 - e^{-\gamma t})^2. \end{aligned} \quad (13)$$

In Ref. 35 we discussed the linear response of our model and its relation to the Anderson-Kubo model. Here we shall focus solely on the higher-order responses that reveal the dynamic

evolution of the two-dimensional coherent excitation lineshape. The third-order response involves phase-matched interactions of the system with a sequence of three laser pulses:

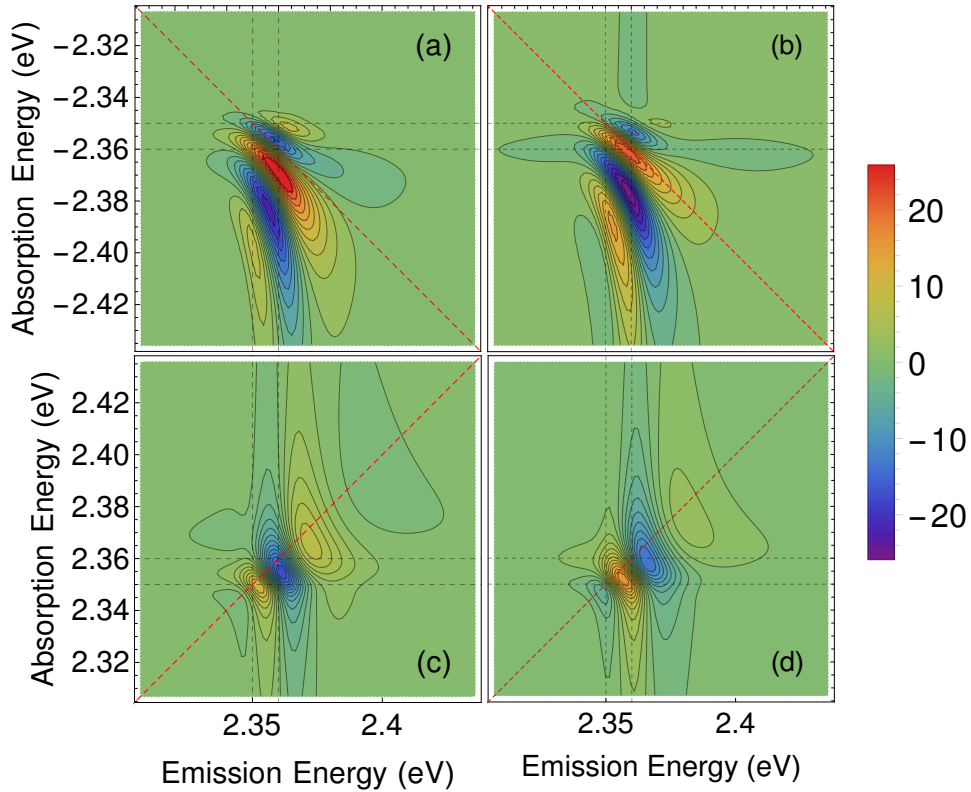


FIG. 3. Theoretical real and imaginary spectra, respectively, of rephasing [(a), (b)] and nonrephasing [(c), (d)] phase matching and at population waiting time $\tau_p = 0$ fs. The vertical false color scale indicated to the right if the figure is in arbitrary units.

$$S^{(3)}(\tau_3, \tau_2, \tau_1) = \langle \mu(\tau_3) [\mu(\tau_2), [\mu(\tau_1), [\mu(0), \rho(-\infty)]]]] \rangle. \quad (14)$$

The times $0 < \tau_1 < \tau_2 < \tau_3$ define the sequence of the time-ordered interactions in Fig. 2. The expressions for these can be evaluated using the standard rules for double-sided Feynman diagrams (Fig. 2, c.f. Ref. 44) representing various optical paths that for a given pathway take the form

$$R_n(\tau_1, \tau_2, \tau_3) = -\left(\frac{i}{\hbar}\right)^4 \mu^4 e^{-i(\omega_0 + n_0 \gamma_1)(\pm \tau_3 \pm \tau_2 \pm \tau_1)} \left\langle \exp \left[i \gamma_1^2 \sum_{j=1}^3 (\pm)_j \int_0^{\tau_j} N(s) ds \right] \right\rangle \quad (15)$$

$$= n_0^2 \exp \left[-i(\omega_0 + n_0 \gamma_1) \sum_{j=1}^3 (\pm)_j \tau_j \right] \times \exp[-i \gamma_1 g_1(\pm \tau_1, \pm \tau_2, \pm \tau_3)] \exp \left[-\frac{\gamma_1^2}{2} g_2(\pm \tau_1, \pm \tau_2, \pm \tau_3) \right]. \quad (16)$$

The sign function $(\pm)_j$ takes “+” and “-” depending upon the sign of the photon wavevector entering or leaving the system. Note that $g_1(\tau_j) = 0$ when the system is initially prepared in the ground state since $N_0 = 0$. Fig. 2 shows the most relevant diagrams for the rephasing (−) and non-rephasing (+) optical response.

It is important to notice that the exciton-exciton interaction term γ_1 , and hence the screening due to exciton-lattice interactions, appears in three distinct places in the third-order re-

sponses. First, as a frequency shift due to self-interactions between the bright excitons. Second, as a frequency shift due to interactions of bright excitons with the evolving background population density. Third, as the leading contribution to the lineshape. In addition, the third term involving $g_2(t)$ carries the influence of the initial conditions (via σ_{N_0}). The effect of many-body exciton-exciton scattering thus leads to time-evolving EID processes. Given these observations, we expect that the homogeneous linewidth will evolve with population

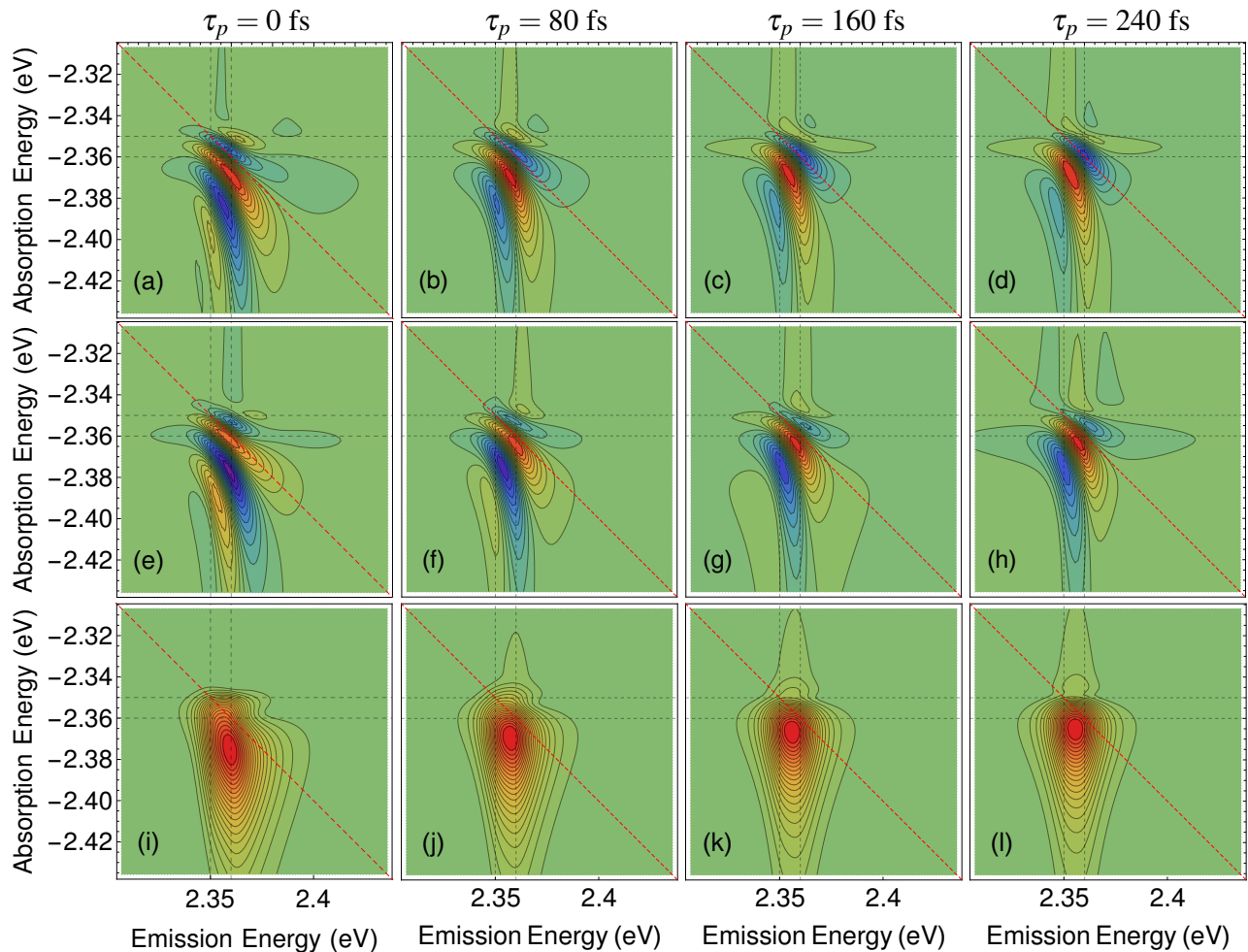


FIG. 4. (a)–(d): Real parts of theoretical rephasing spectra at population times τ_p indicated at the top of each panel. (e)–(h): Corresponding imaginary parts of the spectrum. (i)–(l): The norm (absolute value) of the optical response.

time, dictated by the evolution of $g_2(t)$.

III. TWO-DIMENSIONAL COHERENT SPECTROSCOPY

A. Predictions from the stochastic model

Having established the mathematical model, let us briefly recapitulate some of its features. First, we started by assuming that the background population dynamics give rise to a stochastic process $N(t)$ that enters into the Heisenberg equations of motion for the system operators (Eq. 3). In particular, we assumed that $N(t)$ corresponds to an overdamped Brownian oscillator and that at time $t = 0$ there is a non-stationary population of background excitations. These two mathematical assumptions can be relaxed to some extent if one has a more detailed description of the spectral density of the background process and the initial background population. Secondly, we assume that averages over exponential terms can be evaluated using the cumulant expansion. What then follow are the mathematical consequences as expressed in terms of

the spectral responses of the model. In Ref. 35 we explored the linear response, especially as compared to the Anderson-Kubo model.^{31,32} The key features of our model include:³⁵

1. *Blocking*: Increasing the initial background exciton density suppresses the peak absorption intensity.
2. *Energy shift*: The peak position shifts to the blue with increasing background population due to increased Coulombic interactions.
3. *Broadening*: The spectrum acquires a log tail extending to the blue due to the dynamical evolution of the background. This feature appears in the 2D coherent spectroscopy as an asymmetry along the absorption axis and as phase scrambling in the rephasing and non-rephasing signals (see Figs. S4 and S5 in the Supplemental Material of ref. 27 for the exciton-density-dependent line-shapes at $\tau_p = 0$).
4. *Biexciton formation*: The peak is split by $\gamma_1/2$ corresponding to the biexciton interaction.³⁷

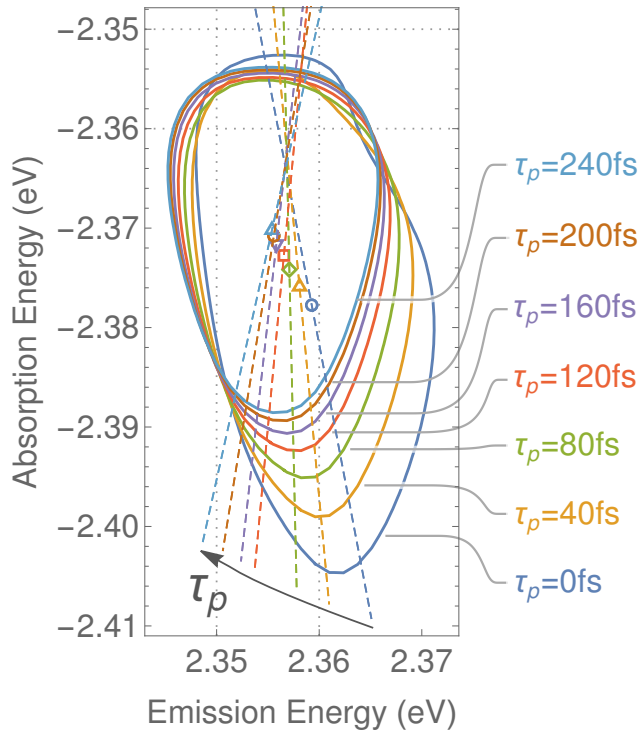


FIG. 5. Exciton 2D coherent lineshape contour at half-maximum intensity as a function of population waiting time derived from the theoretical rephasing absolute spectral evolution in Fig. 4. The center of mass and one of the principle axes are shown for each contour.

These effects are consistent with experimental observations and theoretical models of 2D semiconductors and transition metal dicalcogenides.²⁸

Figs. 3, 4, and 5 correspond to the rephasing and non-rephasing behavior of theoretical model as parametrized to approximate the excitons in the 2D metal-halide perovskite system studied in the experimental investigations, which we shall describe later in this section. The parameters used to produce these spectra are given in Table I. The two pairs of gray dashed lines correspond to the bare exciton energy at $\hbar\omega_0 = 2.35$ eV and the dressed exciton energy at $\hbar\omega_0 + \gamma_1/2 = 2.36$ eV. Fig. 3 gives the rephasing (a,b) and non-rephasing (c,d) spectra computed at $\tau_p = 0$. Two features highlighted above are immediately striking in the modelled 2D spectra. Both the asymmetry of the signals as well as the lineshape inversion of the real and imaginary spectral components can be traced specifically to terms within the response functions in Eq. 16 that depend upon the transient background relaxation and exciton self-interactions.

Both the phasing and asymmetry evolve with increasing population time as shown in Fig. 4(a-l). Importantly, the rephasing signal evolves being dispersive at $\tau_p = 0$ to absorptive at longer times. The non-rephasing signal [Fig. 4(e-h)] has complementary behavior, evolving from absorptive to dispersive. Figs. 4(i-l) give the absolute value of the total response as it evolves over τ_p . The peak is displaced from the diagonal and its position as well as the linewidth evolves over τ_p .

Description	Symbol	Value
bare exciton energy	$\hbar\omega_0$	2.35 eV
noise variance	σ^2	0.0025 fs ⁻¹
relaxation rate	γ	0.01 fs ⁻¹
exciton/exciton interaction	γ_1	20 meV
avg. init. background density	N_0	2 per unit volume
init. background variance	σ_{N_0}	0.35 per unit volume

TABLE I. Parameters used in the theoretical model to produce Figs. 3, 4, and 5.

In Fig. 5 we extract the contour corresponding to the half-maximum intensity at various indicated τ_p population times. Superimposed over each contour is one of the principal axes of the contour scaled according to its magnitude. The central points are the geometric centers of contours. This analysis clearly shows that the peak systematically narrows, rotates, and distorts as the exciton co-evolves with the background population. Moreover, the center peak shifts by about 10 meV towards the red in both absorption and emission spectral dimensions as Coulombic interactions with the evolving background are diminished — this phenomenon is known as excitation-induced shift.¹⁰ The lineshape evolution predicted by the stochastic model is due to $g_1(t) \neq 0$. The early-time blue shift as well as more rapid dephasing arise from many-body effects contained within g_1 ; as this function decays these effects dissipate as shown in Fig. 5. We note that in equation 16, if we set $g_1 = 0$ the coherent response functions reduce to a stationary background, and the lineshape evolution in Fig. 5 would not arise — see also reference 35.

It should be noted, however, that we assume here that the initial background excitation is broad compared to its fluctuations about a stationary state. Starting from the opposite regime, one can obtain dynamic broadening (rather than narrowing) as the system relaxes to the stationary state. We specifically choose these conditions to best represent the experimental conditions of an ultrafast experiment with ~ 20 fs pulses.

In order to test the predictions of the non-stationary model described above, we have carried out two-dimensional coherent measurements on (PEA)₂PbI₄ (PEA = phenylethylammonium) — a multiple-quantum-well-like single-layer metal-halide perovskite derivative (see Fig. 1(c)). We choose this material to test the theoretical framework developed above because of its susceptibility to strong many-body effects^{27,37,45} and dynamic exciton-lattice coupling that drives their dynamics.^{30,36,38,39} To further examine EID in this material, we dissect the population-time-resolved nonlinear coherent optical lineshape of the family of exciton polarons³⁰ by means of two-dimensional (2D) coherent spectroscopy.⁴⁶ Importantly for this work, the 2D coherent optical lineshape permits separation of the homogeneous and inhomogeneous contributions to the linewidth,^{33,34,47} and is therefore an appropriate technique to spectrally and temporally resolve dephasing rates, which we exploit here to quantify EID dynamics. We have discussed the linear spectral lineshape of (PEA)₂PbI₄ in references 36 and 37, and here we summarize it in sec-

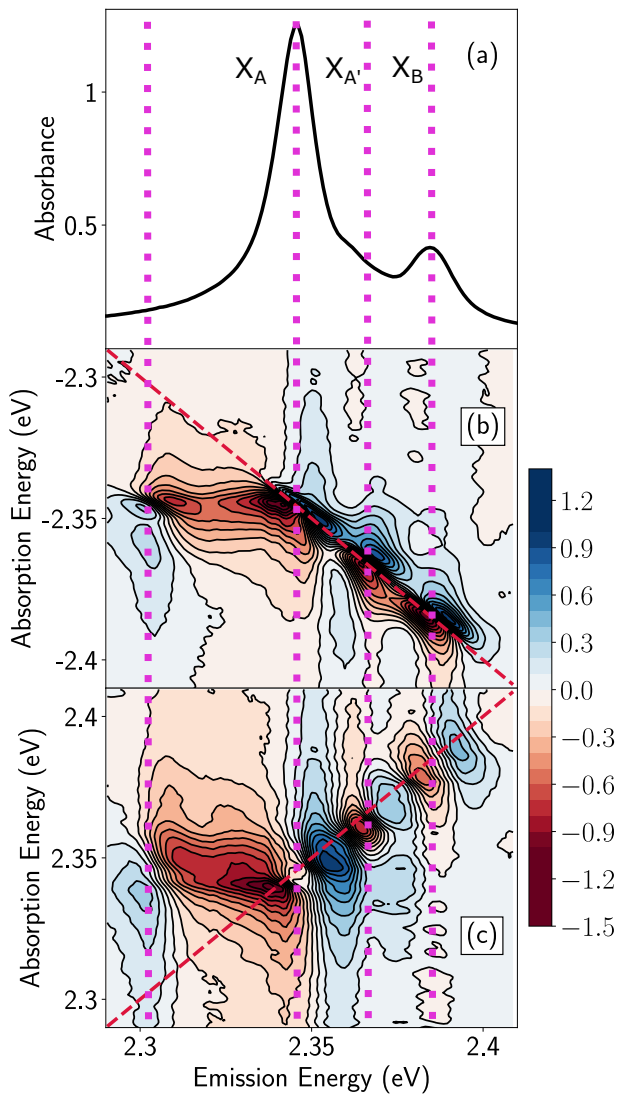


FIG. 6. (a) Linear absorption spectrum of $(\text{PEA})_2\text{PbI}_4$ at 5 K. Real part of the corresponding rephasing (b) and non-rephasing (c) spectra at a population time of $\tau_p = 0$ fs. The bar to the right of the figure displays the vertical false color scale in arbitrary units.

tion III B. We will then discuss the 2D spectral lineshapes of $(\text{PEA})_2\text{PbI}_4$ in section III C. Specifically, we will present the experimentally observed dispersive lineshape as a signature of EID, which we had suggested previously in Ref. 27. We will show that such a lineshape evolves into absorptive form with population time, as a consequence of $g_2(t)$ in the response function which is quenched due to the increased screening of exciton-exciton interactions.

B. Linear absorption lineshape

We display the linear absorption spectrum of $(\text{PEA})_2\text{PbI}_4$ measured at 5 K in the region of exciton absorption, in Fig. 6(a). It has been reported extensively that this spectrum displays structure consisting of multiple reso-

nances.^{30,36,37,48–52} We have argued previously that the primary photoexcitations in two-dimensional hybrid metal-halide perovskite derivatives are a family of exciton polarons,³⁰ with exciton binding energies differing by ~ 40 meV,³⁶ and each with distinct phonon dressing.³⁸ Here, we focus on the two primary transitions labelled X_A and X_B , but we also highlight an additional shoulder of X_A , labelled $X_{A'}$. We had initially hypothesized that $X_{A'}$ is the envelope of replicas in a vibronic progression with origin X_A ,³⁶ but we then subsequently found that its elastic scattering rate is distinct from X_A and X_B ,²⁷ indicating it to be another distinct state within the spectral bandwidth of the excitonic transitions. We highlight that this spectral structure is general to other derivatives with different organic cations, including ones that induce lattice distortions⁵³ that modulate the central exciton binding energy,^{36,54} and the relative intensities of the transitions, but not the energy spacing in the spectral structure.^{30,36}

C. Time-resolved 2D coherent excitation lineshape

We next consider the complex 2D coherent excitation spectrum to quantify the consequences of EID in the nonlinear lineshape. We have previously reported that the multiple excitons identified in Fig. 6(a) display strong many-body effects, manifested via the presence of stable biexcitons³⁷ and the dominance of EID signatures on the homogeneous linewidth.²⁷ We have observed that X_A and X_B display different dependence of EID on exciton density and on temperature²⁷ and have interpreted these phenomena as indicative of specific dynamic Coulomb screening of X_A and X_B by different polaronic dressing phonons.³⁸

Shown in Figs. 6(b) and 6(c) are the real parts of two different coherent excitation pathways; the time-ordering of the three optical pulses in the experiment and phase-matching conditions define the specific excitation pathways, based on which *rephasing* [Fig. 6(b)] and *non-rephasing* [Fig. 6(c)] spectra are obtained.⁴⁶ In the rephasing experiment, the pulse sequence is such that the phase evolution of the polarization after the first pulse and the third pulse are of opposite sign, while in the non-rephasing experiment, they are of the same sign (see equation 16 and Fig. 2). Both measurements shown in Fig. 6 are taken at a population waiting time $\tau_p = 0$ fs and an excitation fluence of 40 nJ/cm^2 , which corresponds to an exciton density in which we have identified effects of elastic exciton-exciton scattering.²⁷ Corresponding diagonal spectral features at the energies of X_A , $X_{A'}$ and X_B (indicated by the magenta vertical dotted-lines in Fig. 6) are observed, both in rephasing and non-rephasing spectra. Apart from these diagonal peaks, we observe an off-diagonal excited-state absorption feature (opposite phase with respect to the diagonal features) corresponding to a correlation between the absorption energy of X_A and emission energy ~ 2.3 eV, which has no corresponding diagonal signal. We have assigned this cross-peak to a biexciton resonance.³⁷

From the norm of the rephasing spectrum at zero time [not shown in Fig. 6 but shown below in Fig. 7(i)], one can extract the homogeneous and inhomogeneous linewidths via

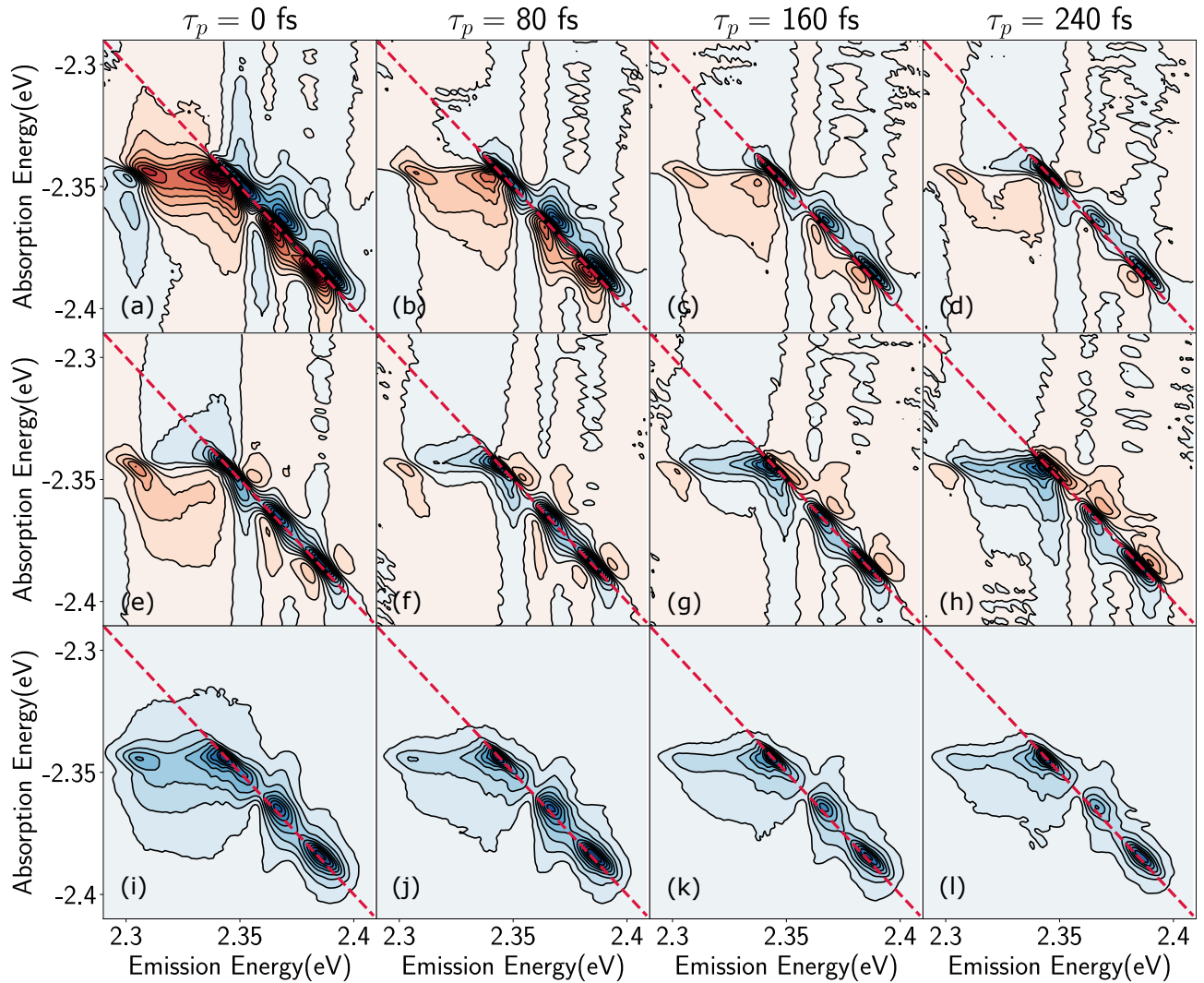


FIG. 7. (a)–(d): Real parts of experimentally measured rephasing spectra at population times τ_p indicated at the top of each panel, measured at 5 K. (e)–(h): Corresponding imaginary parts of the spectrum. (i)–(l): The norm (absolute value) of the optical response. All spectra components are plotted in the same relative vertical color scale to facilitate comparison of the time-dependent signal.

a global analysis of the diagonal and the anti-diagonal lineshape.^{33,34} In reference 27 we reported that the homogeneous linewidth (γ_0) in the absence of excitation induced dephasing (zero-density limit) is approximately 2 meV for all the observed excitonic resonances, that implies a dephasing time $T_2^* \sim 500$ fs.⁵⁵ This linewidth is comparable to the inhomogeneous width of ~ 6.5 meV, placing this system firmly in a dynamic disorder regime. Upon increasing exciton density, the homogeneous linewidth derived from the $\tau_p = 0$ fs spectrum increases due to EID arising from many-body elastic scattering. As mentioned earlier in this section, by quantifying the contribution of EID to the homogeneous linewidth, we have concluded that X_A and X_B demonstrate distinct exciton-exciton scattering rates, which we attributed to their peculiar phonon dressing³⁸ leading to a specific dynamic Coulomb screening of their nonlinear coupling.

In Ref. 27, we considered the norm of the rephasing spectrum at $\tau_p = 0$ fs; however upon close inspection of Fig. 6, we

notice that the real part of the lineshape in Fig. 6 displays dispersive shape, i.e. derivative shape about the peak energy, both for diagonal and off-diagonal resonances, in both the rephasing and non-rephasing spectrum. Note the sign-flip for the off-diagonal feature, which is consistent with its assignment to the excited state absorption to the biexcitonic state. Similarly, the imaginary part of the spectra (not shown in Fig. 6 but shown below in Fig. 7) display an absorptive lineshape. The theoretical spectra shown in Fig. 3 suggest that such dispersive lineshapes are a consequence of many-body correlations. In the latter's absence, the lineshape should be purely absorptive. The spectra in Fig. 6 therefore reveal phase mixing due to many-body Coulomb correlations responsible for EID, as has been reported in semiconductor quantum wells.²² In fact, we have demonstrated in Ref. 27 that the EID dominates the non-linear response in the employed pump fluence range. These phenomena are reproduced by the 2D coherent spectra predicted by our stochastic theory, as shown in Fig. 3.

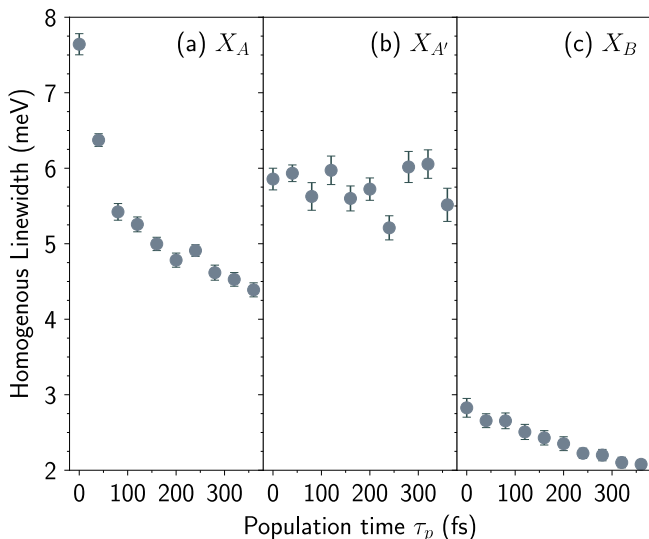


FIG. 8. Homogeneous linewidths obtained from the lineshape analysis of the absolute value of the rephasing spectra (see reference 27) plotted as a function of the population time for (a) X_A , (b) $X_{A'}$ and (c) X_B exciton lines shown in Fig. 6(a).

The evolution of the rephasing lineshape shown in Fig. 6(b) with population waiting time τ_p is displayed in Fig. 7. The top row displays the real part of the spectrum at different values of τ_p , the middle row the imaginary component, and the bottom row the norm (absolute value) of the complex spectrum. We observe that the phase scrambling phenomenon displayed in the $\tau_p = 0$ fs spectrum [Fig. 6(b)] dissipates within $\tau_p \leq 240$ fs: the real component of the spectrum evolves from an initially dispersive [Fig. 7(a)] to absorptive [Fig. 7(d)] lineshape, while that of the imaginary part evolves from absorptive [Fig. 7(e)] to dispersive [Fig. 7(h)] character. We note that although the evolution of the real and imaginary components of the complex lineshape is substantial over this ultrafast time window, the population decay of the diagonal features for X_A and X_B is weak, observed via the modest evolution of the total intensity in Fig. 7(i)–(l). The decay of the $X_{A'}$ diagonal peak and the biexciton cross peak appears more substantial.

The marked evolution of the complex lineshape is also predicted by the stochastic theory as evidenced by the theoretical spectra presented in Fig. 4. Recalling the arguments presented in Sec III A, such a dynamic is fundamentally driven by the exciton-exciton interactions that are time dependent due to the evolving background population. While the theory also predicts asymmetry in the lineshapes, non-negligible inhomogeneous effects, which are not considered in theory yet present in the experimental spectra prevents the observation of clear asymmetry.

We also highlight the reduction in the total linewidth of the each diagonal exciton resonance in the absolute value of the response shown in Fig. 7(i)–(l) with population time. Inspection of these spectra reveal dynamic narrowing of X_A and X_B , primarily along the anti-diagonal spectral axis. It is more difficult to visually ascertain the linewidth evolution of $X_{A'}$ and the biexciton cross peak given the non-negligible decay over

this time period. The dynamic line narrowing in Fig. 7 has also been predicted by the theory, again due to the loss of dephasing pathway in the form of EID. This phenomenon reflects the spectral evolution predicted in 5, which highlights the dynamic line narrowing.

To quantify the measured dynamic line narrowing, we display in Fig. 8 the homogeneous linewidth as extracted in reference 27 as a function of population time τ_p . This is extracted by a global analysis of the diagonal and the anti-diagonal lineshape as developed in references 33 and 34: in the limit of similar homogeneous and inhomogeneous widths as is the case in this material,^{27,36,37} the diagonal lineshape follows a Voigt profile, while the anti-diagonal spectrum is the product of a Gaussian and complementary error function, but both diagonal and anti-diagonal widths depend on the dephasing parameter. By this analysis, Fig. 8 shows that the linewidth of X_A reduces most drastically, but that of X_B also reduces over a typical time window, while $X_{A'}$ displays no line narrowing. We note that in reference 27, we reported that X_A has a stronger density dependence of EID than X_B , which is consistent with the observation derived from Figs. 8(a) and 8(c). We have found X_B to be more strongly displaced along phonon coordinates involving octahedral twist in the plane of the inorganic layer, and out of plane scissoring of the Pb—I—Pb apex.³⁸ Interestingly, the homogeneous linewidth of X_A displayed thermal broadening by a dominant phonon mode on the inorganic plane, while the thermal broadening mechanism for X_B involved a phonon with motion involving the organic cation.³⁷ The stronger exciton-phonon coupling implies that X_B is more susceptible to dynamic screening than X_A , which is consistent with the data in Fig. 8 and reference 27. Furthermore, the linewidth of $X_{A'}$ displayed weaker, non-Boltzmann temperature dependence.²⁷ Finally, we point out that the asymptotic value of the homogeneous linewidth for X_A , $X_{A'}$, and X_B tends towards the low-exciton-density linewidths that we reported in reference 27.

The linewidth of $X_{A'}$ remains relatively constant over the probed population time. While this might initially suggest that this resonance is immune to EID effects, we note that the real part of the rephasing spectrum associated to this particular transition exhibits a dispersive lineshape at all population times, consistent with the initial lineshapes of X_A and X_B . This indicates the clear presence of EID effects, as also confirmed by the density dependent linewidth previously published in Ref 27. The trend shown in Fig 8(b), on the other hand, suggests that the inter-exciton scattering does not evolve with the population time, at least within the probed time range. Inspection of the the lineshape, however, suggests that the dispersive lineshape of the real part is preserved at all population times, suggesting $X_{A'}$ is subjected to EID over a much longer period of time than the other two resonances. Following the arguments developed by the theory in this paper, this implies the presence of a background exciton population that contributes to the scattering of $X_{A'}$ and whose stochastic evolution is that of the background of the other two resonances. This reiterates our assignment of the multiple resonances within the spectral structure to excitonic states of distinct character and possibly specific origin.³⁰

D. Consequences for the exciton spectral structure

The origin and nature of the spectral finestructure of the excitonic transition — the presence of distinct resonances such as X_A , $X_{A'}$ and X_B — has been under discussion.⁵² Early works on 2D hybrid metal-halide perovskites suggested that the spectral structure is the outcome of degeneracy-lifting processes driven by spin-exchange interactions ubiquitous to lead-based semiconductors. Even though the spin-exchange energy was estimated to be of the same order magnitude as the energy spacing within the finestructure,⁵⁶ Kataoka et al.,⁵⁷ and more recently Urban et al.,⁵⁸ noted an indiscernible difference in the diamagnetic shift of each of the resonances with applied magnetic field. Alternatively, a more *chemical* perspective was also suggested in which the structure was assigned to a vibronic progression within a single exciton state.^{51,58} This was particularly highlighted in $(\text{PEA})_2\text{PbI}_4$, where Urban et al.⁵⁸ and Straus et al.⁵⁹ have identified a vibrational mode at about 40 meV in the off-resonance Raman spectrum associated to the motion of the phenylethyammonium cation. We underline, however, that in order to unambiguously establish the vibronic nature, it is essential to measure the resonant Raman spectrum, which in fact has dominant contribution from the phonon modes of the inorganic lattice. We have reported that this type of measurement over a lower frequency range reveals distinct displacements along different phonon modes for X_A and X_B .³⁸ Moreover, we highlight that similar, if not the same spectral structure, is observed even in other 2D hybrid metal-halide perovskite derivatives with other organic cations, further suggesting that the spectral structure is unlikely to be vibronic in nature.

We have presented arguments in Ref. 30 as to why we consider that such an interpretation of a vibronic progression for the spectral structure in Fig. 6(a) does not explain a series of experimental observations, including distinct polaronic dressing of X_A and X_B ,³⁸ distinct screening of EID for these excitons,²⁷ and distinct biexciton binding.³⁷ We consider that the clearly peculiar behavior of X_A and X_B in Fig. 8 adds to the body of work that establishes these excitons as a family of distinct but correlated excitons with strong polaronic character.

E. Summary of phenomenology and relationship to predictions from stochastic theory

We summarize the phenomenology presented in ref. 27 and in section III C pertaining to EID effects in the 2D coherent lineshape evolution in $(\text{PEA})_2\text{PbI}_4$.

- The $\tau_p = 0$ rephasing absolute spectrum displays homogenous linewidth that depends on exciton density, with X_A , $X_{A'}$, and X_B displaying distinct density dependence.²⁷ Furthermore, exciton-exciton scattering is activated by phonons on the lead iodide plane for X_A but by motion of the organic cation for X_B , while $X_{A'}$ displays relatively weaker thermal broadening.²⁷ We interpreted these distinct behaviors as indicative of peculiar

screening by the lattice for each exciton polaron.³⁸

- The model predicts a lineshape asymmetry, manifested both in the linear (ref. 35) and nonlinear (Fig. 3) spectrum by a tail to higher energy that depends on the background-exciton density N_0 . This asymmetry is evident in the exciton-density dependence of the $\tau_p = 0$ rephasing lineshape measured experimentally (shown as Supplemental Material in ref. 27).
- Both the $\tau_p = 0$ rephasing and nonrephasing spectra display real and imaginary spectra with inverted lineshape: the real component displays dispersive lineshape while the imaginary one is absorptive (Figs. 6 and 7). This phenomenon is predicted by the stochastic model and arises from the background evolution from the g_1 term (Fig. 3).
- This lineshape inversion dissipates over an ultrafast timescale in which the homogeneous linewidth decreases (Figs. 7 and 8). The dynamics of the lineshape evolution are once again distinct for the different excitons. The linewidth evolution is predicted by the theory, and is ascribed to the time dependence of terms that arise due to EID effects (Figs. 4 and 5). In the situation of broadband excitation in which the initial distribution of exciton energies is broad, the model distinctly predicts dynamic line narrowing, but it also predicts dynamic line broadening in situations of narrow-band excitation (not shown in this manuscript).

The microscopic model developed here captures the essential EID physics and opens new opportunities for novel, detailed understanding of many-body exciton physics and of how system-bath dynamics contribute to non-linear spectral behavior. We note that the theoretical model considered in the first part of the manuscript lacks some of the necessary ingredients to reproduce rigorously the experimental lineshapes, such as spin-exchange and polaronic effects. In spite of this limitation, we have qualitatively identified the physical origin of the observed nonlinear lineshape through the stochastic model presented in this article.

IV. DISCUSSION

We present here a joint theoretical and experimental study of excitation induced dephasing that connects the dynamics of an otherwise dark background density of states to the evolution of the 2D coherent spectral lineshape. Such dynamics are input in our analytical model in the form of the spectral density and corresponding stochastic equations of motion of the background population, which dress the quantum operators for the “bright” degrees of freedom. An important feature of our model and its connection to the experimental observation is that the complex and potentially intractable dynamics of the dark variables can be reduced to a single stochastic variable and a few physical parameters that can be directly related: exciton-exciton interactions and density of states. Coupled

with Itô calculus, this provides a powerful analytical tool for interpreting dynamical features in 2D coherent spectra. Furthermore, the approach can be extended to include additional interactions such as polaronic binding and spin-orbit coupling. We reserve inclusion of these physics for future investigation.

Our model predicts that the homogeneous linewidth evolves with population time purely due to the dynamics of many-body correlations. Dynamic line broadening effects in 2D coherent spectra are often interpreted in the context of spectral diffusion.^{46,60} This work demonstrates that in condensed matter systems, competing line narrowing processes due to many-body interactions can complicate such lineshape evolution. We consider that the fact that the stochastic model developed here and in Ref. 35 predicts that the linewidth changes with time (whether it increases or decreases) is in itself a very important result with profound implications in condensed-matter chemical physics.

This stochastic theory as developed here is strictly valid for semiconductors, but it can be readily developed to include further physics appropriate for the description of Moiré excitons in 2D transition-metal dichalcogenide heterostructures,⁶¹ and signatures of ground-state spin-orbit entanglement in the optical conductivity spectrum of quasi-one-dimensional Mott insulators,^{62,63} for example. These are the two optically accessible systems in which many-body interactions are dominant. Appropriate details of these physics can be, in principle, included in the spectral density in equation 5, and the consequences of these on nonstationary spectral behavior can be unravelled via our model.

V. PERSPECTIVE

The spectral density of the environment plays a central role in many complex systems and governs the relaxation and de-coherence of a quantum subsystem. Typically, we treat the environment as being quasi-stationary. The theoretical model presented in this article presents a means to represent the environment as nonstationary, here in the context of exciton-exciton scattering, leading to a rich evolution of the nonlinear coherent exciton lineshape. Our perspective is that there is ample scope to include richer physics in the spectral density, such as an explicit treatment of polaronic effects in materials such as the 2D metal-halide perovskites considered here.³⁰ We consider that this theoretical development presents opportunities to include microscopic understanding of many-body interactions that are dominant in condensed-matter systems on their quantum dynamics.

The theoretical development presented here allows the exploration of the following open questions in chemical physics community: in multi-chromophoric systems such as light harvesting complexes, does sculpting of the spectral density determine sensitively (compared to experimental observables) the evolution of the optical exciton lineshape in 2D coherent excitation spectra? Does the additional microscopic detail contained in the spectral density of the environment matter to capture the observed lineshape evolution? We believe that our theoretical framework can contribute towards this fundamen-

tal understanding.

ACKNOWLEDGEMENTS

We are deeply thankful to Daniele Cortecchia and Annamaria Petrozza for providing the high quality samples for this work. The work at the University of Houston was funded in part by the National Science Foundation (CHE-1664971, DMR-1903785) and the Robert A. Welch Foundation (E-1337). The work at Georgia Tech was funded by the National Science Foundation (DMR-1904293). CS acknowledges support from the School of Chemistry and Biochemistry and the College of Science at Georgia Tech.

DATA AVAILABILITY

The data that support the findings of this study are available from the corresponding author upon reasonable request.

Appendix A: Experimental Methods

1. Sample Preparation

The samples were provided by Dr. Daniele Cortecchia for the work presented in reference 27, which reports measurements taken concurrently with those reported in this article. Thin films of (PEA)₂PbI₄ (thickness of 40 nm) were prepared on sapphire substrates (optical windows 25 × 0.5 mm, Crystran) by spin coating a 0.05 M solution of the perovskite in N,N-Dimethylformamide (DMF). A quantity of 12.5 mg of (PEA)I (Dyesol) was mixed with 11.5 mg PbI₂ (TCI) and dissolved in 500 μL of DMF (Sigma Aldrich, anhydrous, 99.8%). The solution was left to dissolve on a hotplate at 100°C for 1 hr. After exposing the substrate to an oxygen plasma, the solution (kept at 100°C) was spin-coated on the sapphire window at 6000 rpm for 30 s, and the film was annealed on a hotplate at 100°C for 15 minutes. The solution and the film were prepared in a glove-box under a N₂ atmosphere.

2. Two-Dimensional Coherent Excitation Spectroscopy

The pulse train (25 fs, attenuated to a fluence ~ 40 nJ/cm², centered at 530 nm) was generated by a home-built single-pass non-collinear optical parametric amplifier pumped by the third harmonic of a Yb:KGW ultrafast laser system (Pharos Model PH1-20-0200-02-10, Light Conversion) with output pulse train at 1030 nm and a repetition rate of 100 kHz, an output power of 20 W and a pulse duration of 220 fs. Two-dimensional spectroscopic measurements were performed using a home-built, pulse-shaper-based multidimensional spectrometer that passively stabilizes the relative phase of each pulses.⁶⁴ Our implementation is described in detail in ref. 37, albeit with a different ultrafast laser source with much lower

repetition rate. Each beams was independently compressed using chirp-scan⁶⁵ to a pulse duration of 25 fs FWHM, and was characterized using cross-correlated second harmonic frequency resolved optical gating⁶⁶ (SH-XFROG) in a 10 μm -thick BBO crystal placed at the sample position. For details of pulse characterization, including a typical SH-XFROG trace, we refer the reader to reference 27 since the data presented in this manuscript was taken simultaneously as the data presented in that article. The sample was kept at 5 K using a vibration-free cold-finger closed-cycle cryostat (Montana In-

struments).

Appendix B: Correlation Functions

Here we provide the third-order correlation functions have been used in this work. The correlation functions are defined in the same way as in the reference 44. The subscripts “*a*” and “*b*” denote single and double excitation manifolds, respectively.

The correlation functions with rephasing phase matching are

$$\begin{aligned}
 R_{2a}(t_3, t_2, t_1) &= R_{3a}(t_3, t_2, t_1) \\
 &= \exp \left[-\frac{i}{\hbar} (\omega_0 + n_0 \frac{\gamma_1}{2}) (t_3 - t_1) \right] \exp \left[-\frac{i}{\hbar} \frac{\gamma_1 N_0}{\gamma} (e^{-\gamma t_1} + e^{-\gamma(t_1+t_2)} - e^{-\gamma(t_1+t_2+t_3)} - 1) \right] \\
 &\quad \times \exp \left[-\frac{\gamma_1^2 \sigma^2}{4\hbar^2 \gamma^3} \left(-e^{-2\gamma t_1} + 4e^{-\gamma t_1} - 2e^{-\gamma t_2} - e^{-2\gamma(t_1+t_2)} + 4e^{-\gamma(t_1+t_2)} - 2e^{-\gamma(2t_1+t_2)} + 2e^{-\gamma t_3} + 2e^{-\gamma(t_2+t_3)} \right. \right. \\
 &\quad \left. \left. - e^{-2\gamma(t_1+t_2+t_3)} - 4e^{-\gamma(t_1+t_2+t_3)} + 2e^{-\gamma(2t_1+t_2+t_3)} + 2e^{-\gamma(2t_1+2t_2+t_3)} + 2\gamma(t_1 + t_3) - 5 \right) \right. \\
 &\quad \left. - \frac{\gamma_1^2 \sigma_{N_0}^2}{2\hbar^2 \gamma^2} \left(e^{-\gamma t_1} + e^{-\gamma(t_1+t_2)} - e^{-\gamma(t_1+t_2+t_3)} - 1 \right)^2 \right],
 \end{aligned} \tag{B1}$$

and

$$R_{1b}^*(t_3, t_2, t_1) = 2 \exp \left[-\frac{i}{2\hbar} \gamma_1 t_3 \right] R_{2a}(t_3, t_2, t_1). \tag{B2}$$

The correlation functions with non-rephasing phase matching are

$$\begin{aligned}
 R_{1a}(t_3, t_2, t_1) &= R_{4a}(t_3, t_2, t_1) \\
 &= \exp \left[-\frac{i}{\hbar} (\omega_0 + n_0 \frac{\gamma_1}{2}) (t_3 + t_1) \right] \exp \left[-\frac{i}{\hbar} \frac{\gamma_1 N_0}{\gamma} (-e^{-\gamma t_1} + e^{-\gamma(t_1+t_2)} - e^{-\gamma(t_1+t_2+t_3)} + 1) \right] \\
 &\quad \times \exp \left[-\frac{\gamma_1^2 \sigma^2}{4\hbar^2 \gamma^3} \left(-e^{-2\gamma t_1} + 4e^{-\gamma t_1} + 2e^{-\gamma t_2} - e^{-2\gamma(t_1+t_2)} - 4e^{-\gamma(t_1+t_2)} + 2e^{-\gamma(2t_1+t_2)} + 2e^{-\gamma t_3} - 2e^{-\gamma(t_2+t_3)} \right. \right. \\
 &\quad \left. \left. - e^{-2\gamma(t_1+t_2+t_3)} + 4e^{-\gamma(t_1+t_2+t_3)} - 2e^{-\gamma(2t_1+t_2+t_3)} + 2e^{-\gamma(2t_1+2t_2+t_3)} + 2\gamma(t_1 + t_3) - 5 \right) \right. \\
 &\quad \left. - \frac{\gamma_1^2 \sigma_{N_0}^2}{2\hbar^2 \gamma^2} \left(-e^{-\gamma t_1} + e^{-\gamma(t_1+t_2)} - e^{-\gamma(t_1+t_2+t_3)} + 1 \right)^2 \right],
 \end{aligned} \tag{B3}$$

and

$$R_{2b}^*(t_3, t_2, t_1) = 2 \exp \left[-\frac{i}{2\hbar} \gamma_1 t_3 \right] R_{1a}(t_3, t_2, t_1). \tag{B4}$$

REFERENCES

- ¹A. Mysyrowicz, J. Grun, R. Levy, A. Bivas, and S. Nikitine, “Excitonic molecule in CuCl,” *Phys. Lett. A* **26**, 615–616 (1968).
- ²D. Magde and H. Mahr, “Exciton-exciton interaction in CdS, CdSe, and ZnO,” *Phys. Rev. Lett.* **24**, 890 (1970).
- ³J. Grun, S. Nikitine, A. Bivas, and R. Levy, “Luminescence of copper halides excited by a high power laser,” *J. Lumin.* **1**, 241–253 (1970).
- ⁴R. Miller, D. Kleinman, A. Gossard, and O. Munteanu, “Biexcitons in GaAs quantum wells,” *Phys. Rev. B* **25**, 6545 (1982).
- ⁵D. Kleinman, “Binding energy of biexcitons and bound excitons in quantum wells,” *Phys. Rev. B* **28**, 871 (1983).
- ⁶Y. Hu, S. W. Koch, M. Lindberg, N. Peyghambarian, E. Pollock, and F. F. Abraham, “Biexcitons in semiconductor quantum dots,” *Phys. Rev. Lett.* **64**, 1805 (1990).
- ⁷K. Brunner, G. Abstreiter, G. Böhm, G. Tränkle, and G. Weimann, “Sharp-line photoluminescence and two-photon absorption of zero-dimensional

- biexcitons in a GaAs/AlGaAs structure,” *Phys. Rev. Lett.* **73**, 1138 (1994).
- ⁸T. Albrecht, K. Bott, T. Meier, A. Schulze, M. Koch, S. Cundiff, J. Feldmann, W. Stolz, P. Thomas, S. W. Koch, *et al.*, “Disorder mediated biexcitonic beats in semiconductor quantum wells,” *Phys. Rev. B* **54**, 4436 (1996).
- ⁹K. W. Stone, K. Gundogdu, D. B. Turner, X. Li, S. T. Cundiff, and K. A. Nelson, “Two-quantum 2d ft electronic spectroscopy of biexcitons in gas quantum wells,” *Science* **324**, 1169–1173 (2009).
- ¹⁰D. Karaiskaj, A. D. Bristow, L. Yang, X. Dai, R. P. Mirin, S. Mukamel, and S. T. Cundiff, “Two-quantum many-body coherences in two-dimensional fourier-transform spectra of exciton resonances in semiconductor quantum wells,” *Phys. Rev. Lett.* **104**, 117401 (2010).
- ¹¹D. B. Turner and K. A. Nelson, “Coherent measurements of high-order electronic correlations in quantum wells,” *Nature* **466**, 1089–1092 (2010).
- ¹²L. Schultheis, J. Kuhl, A. Honold, and C. W. Tu, “Ultrafast phase relaxation of excitons via exciton-exciton and exciton-electron collisions,” *Phys. Rev. Lett.* **57**, 1635–1638 (1986).
- ¹³A. Honold, L. Schultheis, J. Kuhl, and C. W. Tu, “Collision broadening of two-dimensional excitons in a GaAs single quantum well,” *Phys. Rev. B* **40**, 6442–6445 (1989).
- ¹⁴H. Wang, K. Ferrio, D. G. Steel, Y. Z. Hu, R. Binder, and S. W. Koch, “Transient nonlinear optical response from excitation induced dephasing in GaAs,” *Phys. Rev. Lett.* **71**, 1261–1264 (1993).
- ¹⁵H. Wang, K. B. Ferrio, D. G. Steel, P. R. Berman, Y. Z. Hu, R. Binder, and S. W. Koch, “Transient four-wave-mixing line shapes: Effects of excitation-induced dephasing,” *Phys. Rev. A* **49**, R1551–R1554 (1994).
- ¹⁶Y. Z. Hu, R. Binder, S. W. Koch, S. T. Cundiff, H. Wang, and D. G. Steel, “Excitation and polarization effects in semiconductor four-wave-mixing spectroscopy,” *Phys. Rev. B* **49**, 14382–14386 (1994).
- ¹⁷T. Rappen, U.-G. Peter, M. Wegener, and W. Schäfer, “Polarization dependence of dephasing processes: A probe for many-body effects,” *Phys. Rev. B* **49**, 10774–10777 (1994).
- ¹⁸H. P. Wagner, A. Schätz, R. Maier, W. Langbein, and J. M. Hvam, “Coherent optical nonlinearities and phase relaxation of quasi-three-dimensional and quasi-two-dimensional excitons in $\text{ZnS}_x\text{Se}_{1-x}/\text{ZnSe}$ structures,” *Phys. Rev. B* **56**, 12581–12588 (1997).
- ¹⁹H. P. Wagner, A. Schätz, W. Langbein, J. M. Hvam, and A. L. Smirl, “Interaction-induced effects in the nonlinear coherent response of quantum-well excitons,” *Phys. Rev. B* **60**, 4454–4457 (1999).
- ²⁰J. M. Shacklette and S. T. Cundiff, “Role of excitation-induced shift in the coherent optical response of semiconductors,” *Phys. Rev. B* **66**, 045309 (2002).
- ²¹J. Shacklette and S. T. Cundiff, “Nonperturbative transient four-wave-mixing line shapes due to excitation-induced shift and excitation-induced dephasing,” *J. Opt. Soc. Am. B* **20**, 764–769 (2003).
- ²²X. Li, T. Zhang, C. N. Borca, and S. T. Cundiff, “Many-body interactions in semiconductors probed by optical two-dimensional fourier transform spectroscopy,” *Phys. Rev. Lett.* **96**, 057406 (2006).
- ²³G. Moody, M. E. Siemens, A. D. Bristow, X. Dai, D. Karaiskaj, A. S. Bracker, D. Gammon, and S. T. Cundiff, “Exciton-exciton and exciton-phonon interactions in an interfacial GaAs quantum dot ensemble,” *Phys. Rev. B* **83**, 115324 (2011).
- ²⁴G. Nardin, G. Moody, R. Singh, T. M. Autry, H. Li, F. m. c. Morier-Genoud, and S. T. Cundiff, “Coherent excitonic coupling in an asymmetric double ingaas quantum well arises from many-body effects,” *Phys. Rev. Lett.* **112**, 046402 (2014).
- ²⁵G. Moody, C. K. Dass, K. Hao, C.-H. Chen, L.-J. Li, A. Singh, K. Tran, G. Clark, X. Xu, G. Berghäuser, *et al.*, “Intrinsic homogeneous linewidth and broadening mechanisms of excitons in monolayer transition metal dichalcogenides,” *Nat. Commun.* **6**, 8315 (2015).
- ²⁶E. W. Martin, J. Horng, H. G. Ruth, E. Paik, M.-H. Wentzel, H. Deng, and S. T. Cundiff, “Encapsulation narrows excitonic homogeneous linewidth of exfoliated MoSe_2 monolayer,” (2018), arXiv:1810.09834 [cond-mat.mtrl-sci].
- ²⁷F. Thouin, D. Cortecchia, A. Petrozza, A. R. Srimath Kandada, and C. Silva, “Enhanced screening and spectral diversity in many-body elastic scattering of excitons in two-dimensional hybrid metal-halide perovskites,” *Phys. Rev. Res.* **1**, 032032 (2019).
- ²⁸F. Katsch, M. Selig, and A. Knorr, “Exciton-scattering-induced dephasing in two-dimensional semiconductors,” *Phys. Rev. Lett.* **124**, 257402 (2020).
- ²⁹D. Erkensten, S. Brem, and E. Malic, “Excitation-induced dephasing in 2D materials and van der Waals heterostructures,” ArXiv:2006.08392 [cond-mat.mtrl-sci].
- ³⁰A. R. Srimath Kandada and C. Silva, “Exciton polarons in two-dimensional hybrid metal-halide perovskites,” *J. Phys. Chem. Lett.* **11**, 3173–3184 (2020).
- ³¹P. W. Anderson, “A mathematical model for the narrowing of spectral lines by exchange or motion,” *J. Phys. Soc. Jpn.* **9**, 316–339 (1954).
- ³²R. Kubo, “Note on the stochastic theory of resonance absorption,” *J. Phys. Soc. Jpn.* **9**, 935–944 (1954).
- ³³M. E. Siemens, G. Moody, H. Li, A. D. Bristow, and S. T. Cundiff, “Resonance lineshapes in two-dimensional Fourier transform spectroscopy,” *Optics Express* **18**, 17699–17708 (2010).
- ³⁴A. D. Bristow, T. Zhang, M. E. Siemens, S. T. Cundiff, and R. Mirin, “Separating homogeneous and inhomogeneous line widths of heavy-and light-hole excitons in weakly disordered semiconductor quantum wells,” *J. Phys. Chem. B* **115**, 5365–5371 (2011).
- ³⁵H. Li, A. R. Srimath Kandada, C. Silva, and E. R. Bittner, “Stochastic scattering theory for excitation induced dephasing: Comparison to the Anderson-Kubo lineshape,” ArXiv:2008.09218 [physics.chem-ph].
- ³⁶S. Neutzner, F. Thouin, D. Cortecchia, A. Petrozza, C. Silva, and A. R. Srimath Kandada, “Exciton-polaron spectral structures in two dimensional hybrid lead-halide perovskites,” *Phys. Rev. Mater.* **2**, 064605 (2018).
- ³⁷F. Thouin, S. Neutzner, D. Cortecchia, V. A. Dragomir, C. Soci, T. Salim, Y. M. Lam, R. Leonelli, A. Petrozza, A. R. Srimath Kandada, and C. Silva, “Stable biexcitons in two-dimensional metal-halide perovskites with strong dynamic lattice disorder,” *Phys. Rev. Mater.* **2**, 034001 (2018).
- ³⁸F. Thouin, D. A. Valverde-Chávez, C. Quarti, D. Cortecchia, I. Bargigia, D. Beljonne, A. Petrozza, C. Silva, and A. R. Srimath Kandada, “Phonon coherences reveal the polaronic character of excitons in two-dimensional lead halide perovskites,” *Nat. Mater.* **18**, 349–356 (2019).
- ³⁹F. Thouin, A. R. Srimath Kandada, D. A. Valverde-Chávez, D. Cortecchia, I. Bargigia, A. Petrozza, X. Yang, E. R. Bittner, and C. Silva, “Electron-phonon couplings inherent in polarons drive exciton dynamics in two-dimensional metal-halide perovskites,” *Chem. Mater.* **31**, 7085–7091 (2019).
- ⁴⁰M. Born, “Quantenmechanik der stoßvorgänge,” *Zeitschrift für Physik* **38**, 803–827 (1926).
- ⁴¹J. M. Steele, *Stochastic Calculus and Financial Applications* (2001).
- ⁴²H. von Weizsäcker and G. Winkler, “Ito-Calculus,” (1990).
- ⁴³R. F. Fox, “Stochastic calculus in physics,” *J. Stat. Phys.* (1987), 10.1007/BF01011160.
- ⁴⁴S. Mukamel, *Principles of Nonlinear Optics and Spectroscopy* (Oxford University Press, 1995).
- ⁴⁵Y. Kato, D. Ichii, K. Ohashi, H. Kunugita, K. Ema, K. Tanaka, T. Takahashi, and T. Kondo, “Extremely large binding energy of biexcitons in an organic-inorganic quantum-well material $\text{C}_4\text{H}_9\text{NH}_3)_2\text{PbBr}_4$,” *Solid State Commun.* **128**, 15–18 (2003).
- ⁴⁶M. Cho, “Coherent two-dimensional optical spectroscopy,” *Chem. Rev.* **108**, 1331–1418 (2008).
- ⁴⁷A. Tokmakoff, “Two-dimensional line shapes derived from coherent third-order nonlinear spectroscopy,” *J. Phys. Chem. A* **104**, 4247–4255 (2000).
- ⁴⁸K. Gauthron, J. Lauret, L. Doyennette, G. Lanty, A. Al Choueiry, S. Zhang, A. Brehier, L. Largeau, O. Mauguin, J. Bloch, *et al.*, “Optical spectroscopy of two-dimensional layered $(\text{C}_6\text{H}_5\text{C}_2\text{H}_4\text{-NH}_3)_2\text{-PbI}_4$ perovskite,” *Optics Express* **18**, 5912–5919 (2010).
- ⁴⁹K. Tanaka, F. Sano, T. Takahashi, T. Kondo, R. Ito, and K. Ema, “Two-dimensional Wannier excitons in a layered-perovskite-type crystal $(\text{C}_6\text{H}_{13}\text{NH}_3)_2\text{PbI}_4$,” *Solid State Commun.* **122**, 249–252 (2002).
- ⁵⁰K. Tanaka, T. Takahashi, T. Kondo, K. Umeda, K. Ema, T. Umebayashi, K. Asai, K. Uchida, and N. Miura, “Electronic and excitonic structures of inorganic-organic perovskite-type quantum-well crystal $(\text{C}_4\text{H}_9\text{NH}_3)_2\text{PbBr}_4$,” *Japanese J. Appl. Physics, Part 1* **44**, 5923–5932 (2005).
- ⁵¹D. B. Straus and C. R. Kagan, “Electrons, excitons, and phonons in two-dimensional hybrid perovskites: Connecting structural, optical, and electronic properties,” *J. Phys. Chem. Lett.* **9**, 1434–1447 (2018).
- ⁵²C. M. Mauck and W. A. Tisdale, “Excitons in 2D organic-inorganic halide perovskites,” *Trends in Chemistry* (2019).
- ⁵³D. Cortecchia, S. Neutzner, A. R. Srimath Kandada, E. Mosconi, D. Meggiolaro, F. De Angelis, C. Soci, and A. Petrozza, “Broadband emission in

- two-dimensional hybrid perovskites: The role of structural deformation,” *J. Am. Chem. Soc.* **139**, 39–42 (2016).
- ⁵⁴M. Tremblay, F. Thouin, J. Leisen, J. Bacsa, K. A. Srimath, J. Hoffman, M. Kanatzidis, A. Mohite, C. Silva, S. Barlow, *et al.*, “(4NPEA)₂PbI₄ (4NPEA= 4-Nitrophenylethylammonium): Structural, NMR, and optical properties of a 3 × 3 corrugated 2D hybrid perovskite.” *J. Am. Chem. Soc.* **141**, 4521–4525 (2019).
- ⁵⁵We note that γ , and not 2γ , as defined in ref. 27, is the homogeneous linewidth obtained as a fit parameter from global analysis of the diagonal and anti-diagonal cuts of the norm of the rephasing spectrum.
- ⁵⁶K. Ema, K. Umeda, M. Toda, C. Yajima, Y. Arai, H. Kunugita, D. Wolverson, and J. J. Davies, “Huge exchange energy and fine structure of excitons in an organic-inorganic quantum well material,” *Phys. Rev. B* **73**, 241310(R) (2006).
- ⁵⁷T. Kataoka, T. Kondo, R. Ito, S. Sasaki, K. Uchida, and N. Miura, “Magneto-optical study on excitonic spectra in (C₆H₁₃NH₃)₂PbI₄,” *Phys. Rev. B* **47**, 2010 (1993).
- ⁵⁸J. M. Urban, G. Chehade, M. Dyksik, M. Menahem, A. Surrente, G. Trippé-Allard, D. K. Maude, D. Garrot, O. Yaffe, E. Delporte, *et al.*, “Revealing excitonic phonon coupling in (PE)₂(MA)_{n-1}Pb_nI_{3n+1} 2D layered perovskites,” *J. Phys. Chem. Lett.* (2020).
- ⁵⁹D. B. Straus, S. Hurtado Parra, N. Iotov, J. Gebhardt, A. M. Rappe, J. E. Subotnik, J. M. Kikkawa, and C. R. Kagan, “Direct observation of electron-phonon coupling and slow vibrational relaxation in organic-inorganic hybrid perovskites,” *J. Am. Chem. Soc.* **138**, 13798–13801 (2016).
- ⁶⁰S. T. Roberts, J. J. Loparo, and A. Tokmakoff, “Characterization of spectral diffusion from two-dimensional line shapes,” *J. Chem. Phys.* **125**, 084502 (2006).
- ⁶¹Y. Tang, L. Li, T. Li, Y. Xu, S. Liu, K. Barmak, K. Watanabe, T. Taniguchi, A. H. MacDonald, J. Shan, *et al.*, “Simulation of Hubbard model physics in WSe₂/W₂ moiré superlattices,” *Nature* **579**, 353–358 (2020).
- ⁶²D. Controzzi, F. H. L. Essler, and A. M. Tsvelik, “Optical conductivity of one-dimensional mott insulators,” *Phys. Rev. Lett.* **86**, 680–683 (2001).
- ⁶³J. Schlappa, K. Wohlfeld, K. Zhou, M. Mourigal, M. Haverkort, V. Strocov, L. Hozoi, C. Monney, S. Nishimoto, S. Singh, *et al.*, “Spin-orbital separation in the quasi-one-dimensional Mott insulator Sr₂CuO₃,” *Nature* **485**, 82–85 (2012).
- ⁶⁴D. B. Turner, K. W. Stone, K. Gundogdu, and K. A. Nelson, “Invited article: The coherent optical laser beam recombination technique (colbert) spectrometer: Coherent multidimensional spectroscopy made easier,” *Rev. Sci. Instrum.* **82**, 081301 (2011).
- ⁶⁵V. Lorient, G. Gitzinger, and N. Forget, “Self-referenced characterization of femtosecond laser pulses by chirp scan,” *Optics Express* **21**, 24879–24893 (2013).
- ⁶⁶R. Trebino, *Frequency-resolved optical gating: the measurement of ultra-short laser pulses* (Springer Science & Business Media, 2012).